ELSEVIER

Mechanics of Materials 20 (1995) 273–289

MECHANICS OF MATERIALS

# A modified effective crack-length formulation in elastic–plastic fracture mechanics

Dagmar E. Hauf, David M. Parks, Hyungyil Lee

*Department of Mechanical Engineering, Massachusetts Institute of Technology, Cambridge, MA 02139, USA*

Received 14 December 1993; accepted 2 June 1994

**Abstract**

In examining the performance of standard effective crack-length formulations, the authors noted quantitative accuracy up to "high" fractions of limit load under loading conditions for which the elastic $T$-stress was non-negative, while a pronounced deviation from the corresponding continuum elastic–plastic plane-strain finite-element solutions was seen in shallow-cracked geometries having negative $T$-stress. This trend can be rationalized by noting that, under modified boundary layer ($K_I$ and $T$) loading, the maximum plastic zone radius strongly increases as the $T$-stress decreases from zero (J.R. Rice (1974), *J. Mech. Phys. Solids 22*, 17–26; S.G. Larsson and A.J. Carlsson (1973), *J. Mech. Phys. Solids 21*, 263–277; N.P. O'Dowd and C.F. Shih (1991), *J. Mech. Phys. Solids 39(8)*, 989–1015.) Accordingly, we formulate a *modified effective crack length* to account for the effects of the elastic $T$-stress.

The new formulation consistently extends the load range for which accurate predictions of compliance, $J$-integral, and crack-tip constraint are obtained in several plane strain specimen geometries. The magnitude of influence of the $T$-stress varies with specimen type and relative crack depth. The greatest "improvement" to standard effective crack length approximations occurs in specimens of "moderately" negative $T$-stress.

*Keywords:* Effective crack length; Elastic–plastic fracture mechanics; Modified boundary layer formulation; $T$-stress; Moderate-scale yielding; $J$-integral; Crack-tip constraint

## 1. Introduction

One of the basic assumptions behind the application of linear elastic fracture mechanics (LEFM) to elastic–plastic materials is small-scale yielding (SSY). Under the conditions of SSY, i.e. if the crack-tip plastic zone is *much* smaller than any relevant specimen dimension (cf. ASTM E-399 (1983)), the near-crack-tip stress and deformation fields are characterized by a single parameter, the stress intensity factor $K_I$, and the crack problem can be solved by using a boundary layer (BL) approach. This approach considers a semi-infinite crack in an infinite body and replaces the actual conditions of boundary loading by the asymptotic boundary conditions that

$$\sigma_{ij} = \frac{K_I}{\sqrt{2\pi r}} f_{ij}(\theta) \quad \text{as} \quad r \to \infty, \tag{1}$$

where $r$ and $\theta$ are polar coordinates centered at the crack tip, and $f_{ij}(\theta)$ are universal angular variations of the respective stress components. The magnitude of $K_I$ is taken from the solution of the elastic boundary value problem modeling the actual (elastic–plastic) specimen. The extent to which the near-crack-tip fields of the BL solution and those of an actual specimen agree with each other is an indication of the validity of


*SSDI* 0167-6636(94)00058-1

the $K_I$-based one-parameter characterization of crack-tip fields under SSY conditions.

Linear elastic stress analysis becomes increasingly inaccurate as the inelastic region at the crack tip grows with increasing load magnitude. Based on the work of Hult and McClintock (1956) for a Mode III crack in an elastic/perfectly-plastic material, Irwin (1958) argued that the occurrence of crack-tip plasticity makes the crack behave as if it were longer than its physical size. As a result, the displacements work-conjugate to applied loading are larger, and the secant stiffness is lower than in the elastic case. To account for this difference in macroscopic behavior, Irwin used an effective crack length (ECL) which he defined as the sum of the actual crack size and a plastic zone correction (corresponding to half the radial extent of the plastic zone ahead of the crack tip). In more general terms, the resulting ECL can be written as

$$a_{\text{eff}} = a_o + r_y = a_o + \lambda\left(\frac{K_I}{\sigma_y}\right)^2, \tag{2}$$

where $a_o$ is the actual crack length, $r_y$ is the plastic zone size correction, and $\sigma_y$ is the tensile yield strength. The parameter $\lambda$ is the "plastic zone correction factor", which may, for example, depend on Poisson's ratio, strain hardening exponent, etc., but is independent of the applied load and specimen geometry (Rice, 1974). Commonly used values for $r_y$ and thus $\lambda$ are (Tada et al., 1985)

$$r_y = \frac{1}{2\pi}\left(\frac{K_I}{\sigma_y}\right)^2, \quad \lambda = \frac{1}{2\pi} \quad \text{(plane stress)},$$

$$r_y = \frac{1}{6\pi}\left(\frac{K_I}{\sigma_y}\right)^2, \quad \lambda = \frac{1}{6\pi} \quad \text{(plane strain)},$$

$$r_y = \frac{\pi}{16}\left(\frac{K_I}{\sigma_y}\right)^2, \quad \lambda = \frac{\pi}{16} \quad \text{(Dugdale model)}. \tag{3}$$

Edmunds and Willis (1977) obtained in their work on matched asymptotic expansions in nonlinear fracture mechanics an expression for the plastic zone correction in the form

$$r_y = 2C_1(n)\gamma_{11}^2\varepsilon^2 \tag{4}$$

by comparing their asymptotic expansion for the $J$-integral with the plastically corrected prediction for $J$ up to order $\varepsilon^4$, where $\varepsilon$ is a small loading parameter which is taken as the ratio of the applied stress to the yield strength. $C_1(n)$ in Eq. (4) is a material constant depending on the strain hardening exponent $n$, and its value is determined from the far-field expansion of the elastic–plastic "inner" solution. The term $\gamma_{11}$ can also be expressed as (Edmunds and Willis, 1977)

$$\gamma_{11} = \frac{K_I}{2\sqrt{2\pi}\sigma_y\varepsilon}. \tag{5}$$

By using Eq. (5) in Eq. (4), the plastic zone correction in Eq. (2) is obtained as

$$r_y = \frac{C_1(n)}{4\pi}\left(\frac{K_I}{\sigma_y}\right)^2 = \lambda(n)\left(\frac{K_I}{\sigma_y}\right)^2. \tag{6}$$

Here the plastic zone correction factor $\lambda$ is a function of the strain hardening exponent $n$ through its dependence on the material constant $C_1$. Edmunds and Willis (1986) give an approximate formula for $\lambda(n)$ for a power-law hardening material model with the stress/strain relation $\varepsilon/\varepsilon_y = (\sigma/\sigma_y)^n$ for $\varepsilon \geq \varepsilon_y$ as

$$\lambda(n) \doteq \left(\frac{n-1}{n+1}\right)\lambda|_{n=\infty}, \tag{7}$$

where $\lambda|_{n=\infty}$ is the plastic zone correction factor for the non-hardening response.

For the Dugdale yielding model and a perfectly plastic material, $C_1|_{n=\infty} = \frac{1}{6}\pi^2$ (Edmunds and Willis, 1977). Substituting this value in Eq. (6) gives the plastic zone correction as

$$r_y|_{n=\infty} = \frac{\pi}{24}\left(\frac{K_I}{\sigma_y}\right)^2. \tag{8}$$

This is one-third less than the corresponding Dugdale value given in Eq. (3). For an elastic/perfectly-plastic material satisfying the Mises yield criterion, $C_1|_{n=\infty} = 0.24$ (Edmunds and Willis, 1977), and the non-hardening plane strain plastic zone correction becomes

$$r_y|_{n=\infty} \approx 0.019\left(\frac{K_I}{\sigma_y}\right)^2, \tag{9}$$

which is considerably smaller than the conventional plane strain value in Eq. (3).

Sham (1984) determined a similar value for the plane strain plastic zone size correction factor $\lambda|_{n=\infty} = 0.025$, for a non-hardening material by using the modified variational principle of Hilton and Hutchinson (1971).

LEFM solutions based on plastically-corrected crack lengths can extend SSY results to intermediate scale yielding. Accurate estimates of compliance and $J$-integral are obtained up to higher loads as the effective crack length enters the elastic formulations. The effective value of the elastic $J$-integral, for example, is obtained from

$$J = \frac{K_I^2(a_{\text{eff}})}{E'} = \frac{(\hat{\boldsymbol{k}}(a_{\text{eff}}) \cdot \boldsymbol{Q})^2}{E'}, \tag{10}$$

where $E' = E$ for plane stress and $E' = E/(1-\nu^2)$ for plane strain, $E$ is the Young's modulus, and $\nu$ is Poisson's ratio. $\boldsymbol{Q}$ is the vector of generalized load amplitudes with work conjugate displacements $\boldsymbol{q}$ (Rice, 1972a), and $\hat{\boldsymbol{k}}$ are corresponding stress intensity calibration functions for the generalized loads.[1] Corrections based on Eqs. (2), (9), and (10), however, are only asymptotic approximations of elastic–plastic behavior and typically deviate from continuum solutions at nominal tensile stresses greater than approximately $\sigma_y/2$.

Larsson and Carlsson (1973) performed plane-strain elastic–plastic finite-element analyses on four commonly-employed test specimens exhibiting a variety of crack-tip constraint under SSY conditions and compared their computed plastic zones with the appropriately-scaled plane-strain BL solution. They found significant discrepancies with the BL formulation, even within the range of loads allowed by the ASTM Standard Test Method for Plane-Strain Fracture Toughness of Metallic Materials (E-399). At the maximum permitted load levels, the computed maximum plastic zone sizes for the center-cracked specimen and the double edge-cracked specimen, for example, were greater than that of the BL solution by ~50% and ~25%, respectively. The plastic zones for the different cases would have coincided had the elastic–plastic crack-tip state been determined by $K_I$ alone. Larsson and Carlsson showed that the observed differences in plastic zone sizes of the specimens, loaded to identical "small" $K_I$-levels, are due to specimen-to-specimen differences in the $T$-stress, the second term of the Williams (1957) eigen-expansion of near-crack-tip elastic stress fields. The $T$-stress is not singular as $r \to 0$, but it can alter the elastic–plastic crack-tip stress state, thus *modifying* the crack-tip plastic zone. Like $K_I$, the $T$-stress in Eq. (11) is a function of geometry, loading conditions, and is proportional to the nominal applied stress (Larsson and Carlsson, 1973; Leevers and Radon, 1982; etc.). For instance, in shallow-cracked specimens under predominately tensile loading, the proportionality constant is negative, while deeper-cracked specimens under bending often have a less negative or even positive $T$-stress.

Larsson and Carlsson applied boundary tractions corresponding to the stress fields of the first two terms in the Williams eigen-expansion,

$$\begin{bmatrix} \sigma_{xx}(r,\theta) & \sigma_{xy}(r,\theta) \\ \sigma_{yx}(r,\theta) & \sigma_{yy}(r,\theta) \end{bmatrix} = \frac{K_I}{\sqrt{2\pi r}} \begin{bmatrix} f_{xx}(\theta) & f_{xy}(\theta) \\ f_{yx}(\theta) & f_{yy}(\theta) \end{bmatrix} + \begin{bmatrix} T_{xx} & 0 \\ 0 & 0 \end{bmatrix}, \tag{11}$$

on the same plane strain domain as that in the previous BL solution. The constant term "$T_{xx}$" in Eq. (11) represents the $T$-stress. The *modified boundary layer (MBL) solutions* using this two-parameter description of the loading transmitted to the crack-tip region were essentially in exact agreement with those of each of the corresponding specimens for all loads up to those giving $K_I = 0.6\sigma_y\sqrt{\pi a}$.

Recently, extensive work has been done on two-parameter characterizations of near-crack-tip fields. Betegón and Hancock (1991) analyzed near-crack-tip fields of plane-strain specimens having positive, zero, and negative $T$-stress. Deep within the plastic zone, the crack opening stress profiles (tensile stress distribution on the plane $\theta = 0$ ahead of the crack) of the specimens closely followed those of the corresponding MBL prediction up to large-scale yielding. The MBL family of solutions are strongly affected by the sign and magnitude of the $T$-stress. A substantial reduction of crack-opening stress (relative to SSY) is seen for $\tau < 0$; moderate stress elevation above SSY is observed for $\tau > 0$. Rice (1974), Shih et al. (1993) and Wang (1991) noted a strong variation of plastic zone size with the $T$-stress. Fig. 1, from the work by

[1] These calibration functions are, for example, readily obtained from the handbook of Tada et al. (1985).

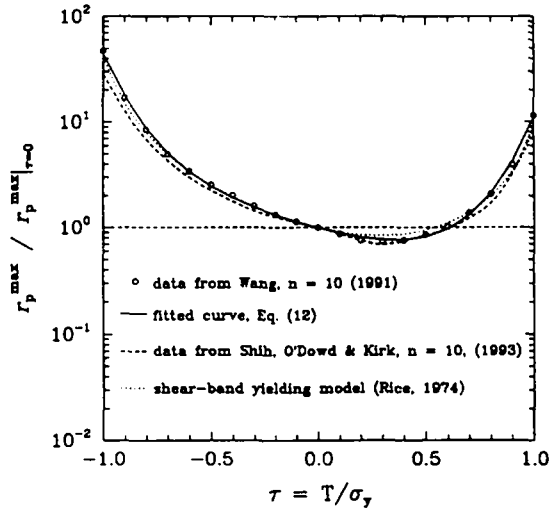


Fig. 1. Variation of maximum plane strain plastic zone size, normalized by the plastic zone size at $\tau = 0$, at various values of $\tau$ (Wang, 1991) in a modified boundary layer formulation.

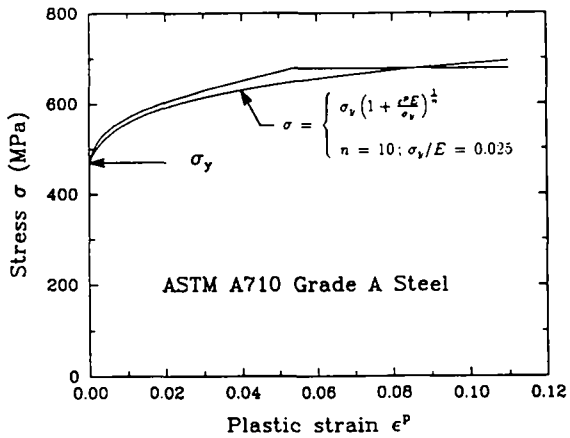


Fig. 2. Engineering stress versus plastic strain curve in uniaxial tension, multi-linearly modeled from experimental data of ASTM A710 Grade A steel and used in flow theory continuum finite-element solutions. Also shown is the power-law fit used in Wang's work (1991) for a moderately hardening material with $n = 10$, and $\nu = 0.3$.

Wang, shows the plastic zone size at various values of $\tau \equiv T/\sigma_y$, normalized by the SSY plastic zone size at $(\tau = 0)$ [2]. The results of the simple shear band yielding model (band shear traction = $\tau_y$, a constant) of Rice (1974) are shown for the purpose of comparison. His results are given in terms of $T$ and the equivalent tensile strength $\sigma_y = \sqrt{3}\tau_y$ with the plastic zone size radius, $r_p$, as

$$r_p = \frac{\pi}{64}\,\frac{\sin^2\phi(1+\cos\phi)}{(1/\sqrt{3}+\tau\sin\phi\cos\phi)^2}\left(\frac{K_I}{\sigma_y}\right)^2. \qquad (12)$$

The angle $\phi$ in Eq. (12) is measured from the crack plane. In practice, $\phi$ in Eq. (12) is an implicit function of $\tau$, $\phi = \hat{\phi}(\tau)$, which is obtained by maximizing $r_p$ with respect to $\phi$ at fixed $\tau$; at $\tau = 0$, this procedure results in $\phi = 70.6°$ (Rice, 1974). Also shown are the results of Shih et al. (1993) for a moderately hardening material ($n = 10$). At $\tau = 0$, $r_p^{max} \sim 0.15(K_I/\sigma_y)^2 \equiv r_p^{SSY}$, which differs only slightly from the generally used nominal plastic zone size, $(1/2\pi)(K_I/\sigma_y)^2$. The maximum plastic zone size grows monotonically with decreasing $\tau$, reaching $\sim 50 r_p^{SSY}$ when $\tau = -1.0$. Positive values of $\tau$ cause the plastic zone size to first decrease, then increase, reaching $\sim 10 r_p^{SSY}$ when $\tau = 1.0$.

In examining the performance of standard ECL formulations in plane strain [Eq. (2) with Edmunds and Willis' non-hardening $\lambda$-value of 0.019, Eq. (9)], the authors obtained quantitative accuracy up to "high" fractions of limit load in geometries and loading conditions for which the elastic $T$-stress was non-negative, while a pronounced deviation from the corresponding continuum elastic–plastic plane-strain finite-element solutions was seen in shallow-cracked geometries having negative $T$-stress. At intermediate load amplitudes, the standard ECL formulations of the geometries with negative $T$-stress produced far less increase in compliance and $J$ than the corresponding continuum solutions.

Based on these observations and on the noted sensitivity of plastic zone size to the sign and magnitude of the $T$-stress, we propose a *modified effective crack length* (MECL) formulation for plane strain by in-

[2] Wang's results are based on a deformation theory plasticity power-law material model with the tensile stress/strain relation

$$\epsilon = \begin{cases} \dfrac{\sigma}{E} & \text{for } \sigma \le \sigma_y \\ \epsilon_y\left(\dfrac{\sigma}{\sigma_y}\right)^n & \text{for } \sigma > \sigma_y;\ 1 < n < \infty, \end{cases}$$

with $\epsilon_y \equiv \sigma_y/E$, and a set of material constants representing a moderately hardening material, namely, $\epsilon_y = 0.0025$, $n = 10$, and $\nu = 0.3$. This relation roughly fits the material data used in the present work (see Fig. 2).

cluding effects of the elastic $T$-stress on plastic zone size into the definition of the effective crack length.

## 2. Formulation

We write the $T$-stress-modified effective crack length in the form

$$a_{\text{eff}} = a + r_{y,\text{mod}} = a + \Lambda(\tau, n)\left(\frac{K_I}{\sigma_y}\right)^2, \tag{13}$$

where $r_{y,\text{mod}}$ is the plastic zone size correction, and $\Lambda(\tau, n)$ is the plastic zone correction factor, which we assume to be a function of the normalized $T$-stress and the strain hardening exponent $n$. In contrast to the plastic zone correction factor $\lambda(n)$ of Eq. (2), $\Lambda(\tau, n)$ is a function of the applied load and specimen geometry through $\tau$. An expression for $\Lambda(\tau, n)$ is proposed in the following.

Referring to Fig. 1, which shows the variation of the plastic zone size with the $T$-stress, the circled data points can be fitted by a fourth-order polynomial. Thus, for $n = 10$:

$$\log_{10}(\rho(\tau, n)) \equiv \log_{10}\left[\frac{r_p^{\max}|_{n=10}(\tau)}{r_p^{\text{SSY}}|_{n=10}}\right] \doteq c_1\tau + c_2\tau^2 + c_3\tau^3 + c_4\tau^4, \tag{14}$$

where $(c_1, c_2, c_3, c_4) = (-0.539, 0.375, 0.236, 0.974)$ are fitting coefficients and $r_p^{\text{SSY}}|_{n=10} = r_p^{\max}|_{n=10}(\tau = 0)$. Analogously to the $K_I$-calibration functions $\hat{k}$, the normalized $T$-stress can be expressed as $\tau = (\hat{t}(a_{\text{eff}}, w) \cdot Q)/\sigma_y$, where $\hat{t}(a_{\text{eff}}, w) = [\hat{t}^N, \hat{t}^M]$ [3] are $T$-stress calibration functions of the specimen under consideration (Wang and Parks, 1992), and $w$ is the width of the specimen. Using second-order weight functions, Sham (1991, 1992) has tabulated values for the $T$-stress calibration functions for various specimens over essentially the entire range of relative crack length $a/w$ ($0.1 \le a/w \le 0.9$). To evaluate $\tau$ in Eq. (14), these values were fitted with polynomial functions (see Appendix B).

We obtain the correction part of the ECL, $r_{y,\text{mod}}$, by assuming that

$$r_{y,\text{mod}} = \beta\, r_p^{\max}(\tau, n) = \beta\,\frac{r_p^{\max}(\tau, n)}{r_p^{\text{SSY}}(n)}\, r_p^{\text{SSY}}(n) \tag{15}$$

$$\equiv \beta\,\rho(\tau, n)\, r_p^{\text{SSY}}(n), \tag{16}$$

where $\beta$ is a scaling factor. Using Eq. (14) in Eq. (15), and noting that $r_p^{\text{SSY}}(n) = g(n)(K_I/\sigma_y)^2|_{\tau=0}$, the plastic zone correction $r_{y,\text{mod}}$, and thus the MECL, can be written as

$$a_{\text{eff}} = a_o + \lambda(n)\,\rho(\tau(a_{\text{eff}}), n)\left(\frac{K_I}{\sigma_y}\right)^2\Bigg|_{\tau=0}, \tag{17}$$

where we have combined the product of constants as $\lambda(n) = \beta g(n)$.

Thus the plastic zone correction factor is given by

$$\Lambda(\tau, n) = \lambda(n)\rho(\tau(a_{\text{eff}}), n). \tag{18}$$

For $\tau = 0$, $\rho = 1$, and Eq. (17) reduces to the standard effective crack length of Eq. (2) with $\Lambda(\tau = 0, n) = \lambda(n)$. This allows us to estimate the value of $\lambda$ from existing ECL solutions. As noted above, Edmunds and Willis (1977) determined a correction factor corresponding to $\lambda|_{n=\infty} = 0.019$ for an elastic/perfectly-plastic material satisfying the Mises yield criterion and $\lambda|_{n=10} = 0.0159$ for a low-hardening material with strain hardening exponent $n = 10$ (Edmunds and Willis, 1986), while Sham (1984) determined a higher non-hardening correction of $\lambda|_{n=\infty} = 0.025$.

Recently Lee and Parks (1995) inferred a value of $\lambda|_{n=10} = 0.0195$. They were working to improve the accuracy of the elastic–plastic line-spring finite element by accounting for effects of the elastic $T$-stress. They compared the numerical results of a SEN specimen of relative crack depth $a/w = 0.5$ (tensile load $N$ versus cracked displacement $\delta^c$; $J$-integral versus $N$) with the continuum elastic–plastic finite-element solution of the same specimen, calibrating the scalar $\lambda$ of, e.g., Eq. (6), until good agreement with the continuum solution was found. Fig. 3 shows a graph of load $N$ versus $\delta^c$ for the SEN specimen at various *constant* values of $\lambda$ (ranging from $\lambda = 0$ to $\lambda = 0.039$ in increments of 0.00975).

Employing Lee and Parks' value for $\lambda|_{n=10}$, the modified effective crack length for $n = 10$ is obtained as

[3] The superscripts $N$ and $M$ denote tension and bending, respectively.

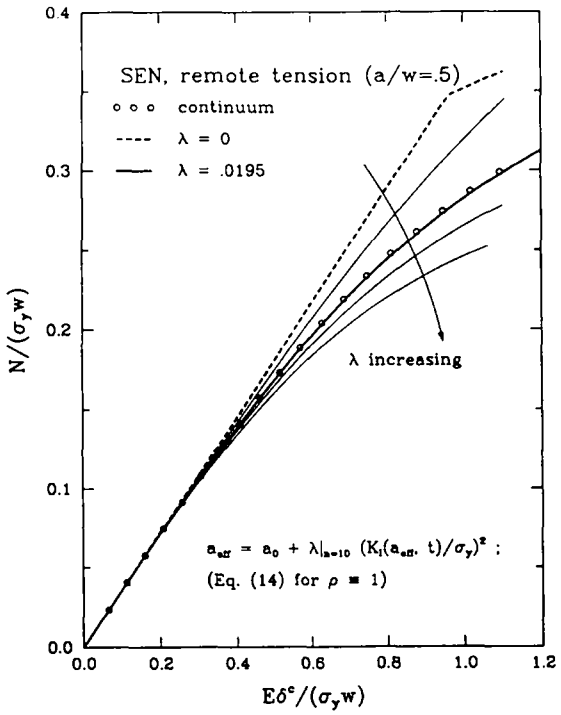


Fig. 3. Normalized axial force $N$ versus cracked displacement $\delta^c$ of a plane-strain SEN of relative crack depth $a/w = 0.5$ under tension (Lee and Parks, 1995).

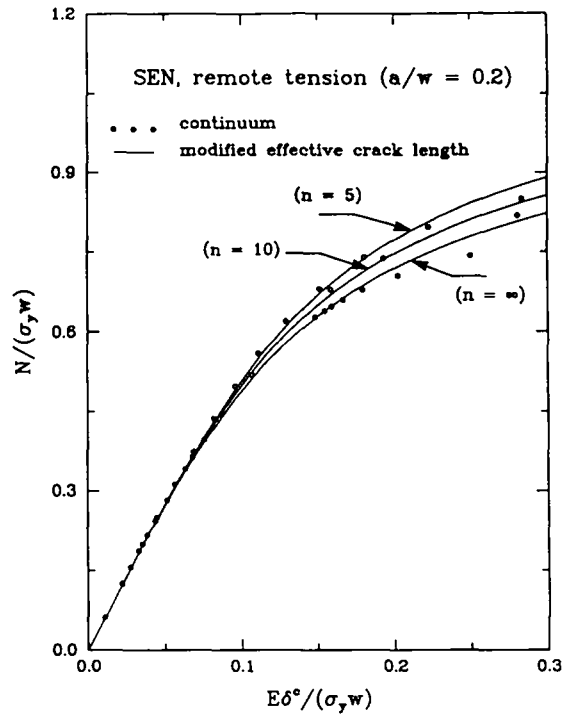


Fig. 4. Normalized axial force $N$ versus cracked displacement $\delta^c$ of a plane-strain SEN of relative crack depth $a/w = 0.2$ for three different strain hardening exponents. Solid lines indicate the modified effective crack length solutions using $\lambda$-values determined with Eq. (7).

$$a_{\text{eff}} = a_o + 0.0195\,\rho(\tau(a_{\text{eff}}))\left(\frac{K_I(\hat{a}_{\text{eff}})}{\sigma_y}\right)^2, \quad (19)$$

where $\hat{a}_{\text{eff}}$ in Eq. (19) corresponds to the effective crack length for the same hardening exponent $n$, but evaluated at $\tau = 0$; i.e.,

$$\hat{a}_{\text{eff}} = a_o + 0.0195\left(\frac{K_I(\hat{a}_{\text{eff}})}{\sigma_y}\right)^2. \quad (20)$$

It is necessary to evaluate an effective $K_I$ and an effective crack length $\hat{a}_{\text{eff}}$ at $\tau = 0$, and hence the corresponding plastic zone size, $r_p^{SSY}$, because of its appearance in the expression for $r_{y,\text{mod}}$, Eq. (15). Evaluation of an effective $K_I$ at $\tau \neq 0$ in Eq. (19) would cause an overcorrection in the MECL solution.

In this context, we tested Edmunds and Willis' proposed formula (Eq. (7)) for the dependence of $\lambda$ on the hardening exponent $n$ for a SEN specimen of relative crack depth $a/w = 0.2$ under remote tension with our MECL formulation. With the Lee and Parks value of $\lambda|_{n=10} = 0.0195$ as the baseline value, we determined values for $\lambda$ for the strain hardening exponents $n = 5$ and $n = \infty$ as $\lambda|_{n=5} = 0.0159$ and $\lambda|_{n=\infty} = 0.0238$, respectively, from Eq. (7). Using these values, curves of normalized load versus cracked displacement were generated and compared to the corresponding continuum solutions. Details of the exact procedure are given in the subsequent sections.

Our results for three hardening exponents, $n = 5, 10$, and $\infty$, are shown in Fig. 4. The MECL solutions for all three $\lambda$-values follow their corresponding continuum solutions well, particularly in the region of initial nonlinearity. The results for $n = 5$ and $n = 10$ are slightly better than those for the non-hardening case. However, Eq. (7) seems acceptable in predicting the variation of the plastic zone correction factor with $n$. The value $\lambda|_{n=10} = 0.0195$ corresponds to a non-hardening value of $\lambda|_{n=\infty} = 0.0238$, which is very close to Sham's value of $\lambda|_{n=\infty} = 0.025$.

The generalized displacements $\boldsymbol{q}$ which are work-conjugate to generalized loads $\boldsymbol{Q}$ applied to a cracked body can be decomposed into

$$q = q|^{\text{no crack}} + q|^{\text{crack}}, \tag{21}$$

where $q|^{\text{no crack}}$ is the displacement of the uncracked body, and $q|^{\text{crack}}$ is the displacement due to the additional compliance introduced by the presence of the crack. Expressions for the cracked and uncracked contributions to the generalized displacements can be derived from the definition of the elastic $J$-integral as the partial derivative of the complementary strain energy $\Omega$ with respect to the crack length; i.e.,

$$J(Q,a) \equiv \frac{\partial \Omega(Q,a)}{\partial a}, \tag{22}$$

where $\Omega$ is given as a function of the generalized loads and the crack length. As our formulation is based on a deformation theory plasticity, use of the $J$-integral is justified here.

Integration of Eq. (22) from zero to the crack length $a$ gives the cracked and the uncracked contributions to the complementary strain energy:

$$\Omega(Q,a) = \Omega(Q,0) + \int_0^a J(Q,a^*)\,da^*. \tag{23}$$

Finally, employing the definition of the generalized displacements $q$ as the partial derivatives of the complementary strain energy with respect to the generalized loads, we readily identify the "crack" and "no crack" portions of $q$:

$$d\Omega = q(Q,a)\cdot dQ = \frac{\partial \Omega}{\partial Q}\cdot dQ = \left( \underbrace{\frac{\partial \Omega(Q,0)}{\partial Q}}_{q|^{\text{no crack}}} + \underbrace{\int_0^a \frac{\partial J(Q,a^*)}{\partial Q}\,da^*}_{q|^{\text{crack}}} \right) \cdot dQ. \tag{24}$$

Using Eqs. (22) and (10) in Eq. (24) allows us to rewrite the cracked displacement as:[4]

$$q|^{\text{crack}} = \frac{2}{E'} \int_{a^*=0}^{a^*=a} K_{\text{eff}}[Q, a_{\text{eff}}(Q,a^*)] \times \frac{\partial K_{\text{eff}}[Q, a_{\text{eff}}(Q,a^*)]}{\partial Q}\,da^*. \tag{25}$$

Thus we have derived an energetically consistent expression for the cracked displacement in terms of $a_{\text{eff}}$ which assures the existence of a potential.

Given values of $q|^{\text{crack}}$, Eqs. (19), (20), and (25) have been solved numerically using the Newton–Raphson method (for definition and derivation of the combined-load Jacobian matrix, see Appendix A) for the SEN specimen in tension and bending, and for the CCP and DEN specimens in tension (see Fig. 6 below) at relative crack depths $a/w = 0.5, 0.35$, and 0.2. Uniform end displacement boundary conditions were imposed on a SEN specimen of relative crack depth $a/w = 0.7$ and total length $l/w = 6$. Eq. (25) was numerically evaluated using 10-point Gaussian integration. The corresponding values of $J(Q, a_{\text{eff}})$ were determined using Eq. (10). Curves of load versus displacement, and $J$-integral versus load were generated. For the pure tension and bending cases, only the cracked displacement was considered; for the uniform end displacement case, the total displacement was obtained, i.e., the displacements of the uncracked specimen were added as

$$\delta^{\text{no crack}} = (l/E'w)N, \quad \theta^{\text{no crack}} = (12l/E'w^3)M.$$

The material considered is ASTM A710 Grade A steel having a Young's modulus of $E = 207$ GPa (see Fig. 2 for tensile stress/strain curve) and Poisson's ratio $\nu = 0.3$. For the continuum finite-element analyses, the material was modeled as isotropic elastic–plastic, obeying $J_2$ flow theory plasticity. Small geometry changes were assumed. The flow strength was given as a function of the equivalent plastic strain, with an initial value of $\sigma_y = 470$ MPa and a saturation value of 677 MPa at plastic strain $\epsilon^p = 0.0538$, which essentially corresponds to a strain hardening exponent of $n = 10$. Thus, in making comparisons of the continuum solutions with the simplified effective crack length formulations, values for $n = 10$ were used in the latter.

[4] The subscript "eff" is used in Eq. (25) to indicate that $K$ is a function of the effective crack length as in Eq. (10).

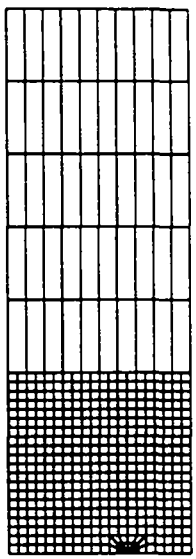

Fig. 5. Finite-element mesh used in analysis, $a/w = 0.35$.

## 3. Elastic-plastic finite-element analysis

The mesh used in the finite-element analysis for $a/w = 0.35$ is shown in Fig. 5. The crack-tip region is modeled by a rectangular domain. Circumferentially, there are eight focused fans of elements, each fan containing four elements radially. The innermost element ring (at the crack tip) is degenerated so one side collapses into a single point at the crack tip. Plane strain, 8-node, reduced integration elements (ABAQUS element type CPE8R) were used. Finite-element analyses were performed on a SEN specimen in tension and bending, and on DEN and CCP specimens in tension, at three different crack depths ($a/w = 0.5$, 0.35 and 0.2). To obtain the "crack" displacement as a function of imposed load, the displacement of the "no-crack" specimen (also obtained by finite-element analysis) was subtracted from the total displacement; i.e., $\delta^c = \delta - \delta^{nc}$. For the uniform-end-displacement loading of the SEN specimen of relative crack depth $a/w = 0.7$ ($l/w = 6$), the total displacement was considered. Taking advantage of symmetry, only half of the SEN specimen was modeled, with symmetry boundary conditions imposed on the plane $y = 0$. For both the DEN and the CCP specimens, symmetry allowed modeling of only one quarter of the specimen (see Fig. 6). For the DEN specimen, symmetry boundary conditions were imposed in the planes $x = -(w - a)$ and $y = 0$, while for the CCP specimen, symmetry boundary conditions were imposed in the planes $x = -a$ and $y = 0$. The coordinates are centered at the crack-tip for both cases (see Fig. 6).

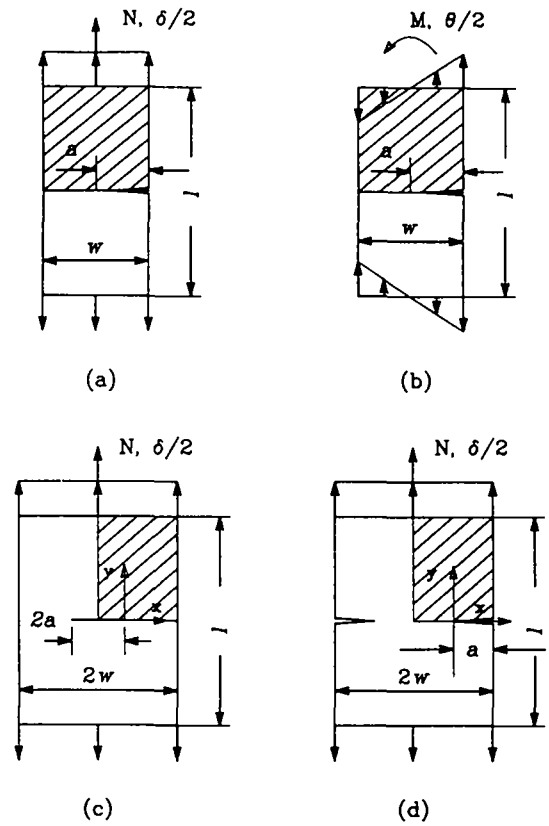


Fig. 6. Specimen geometries (for symmetry reasons only shaded parts are analyzed): single edge-cracked specimen under (a) tension and (b) bending; (c) center-cracked specimen; (d) double edge-cracked specimen.

## 4. Results

Curves of normalized load versus displacement of the three specimens are shown in Figs. 7–11. Figs. 12–16 show normalized values of $J$-integral versus load. Arrows indicate the values of the corresponding non-hardening limit loads (based on $\sigma_y$) obtained from elastic/perfectly-plastic finite-element analyses. The load history of the uniform-end-displacement case is shown in Fig. 17. LEFM solutions and solutions based on the standard effective crack length formulation [Eq. (17) with $\rho \equiv 1$] are shown for the purpose of comparison.

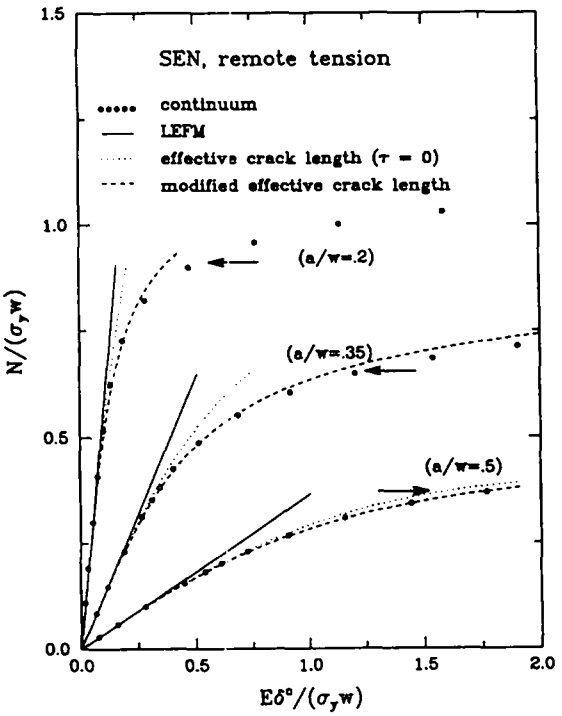


Fig. 7. Normalized axial force $N$ versus cracked displacement for remote tension of a plane-strain SEN. Horizontal arrows denote limit loads based on $\sigma_y$.

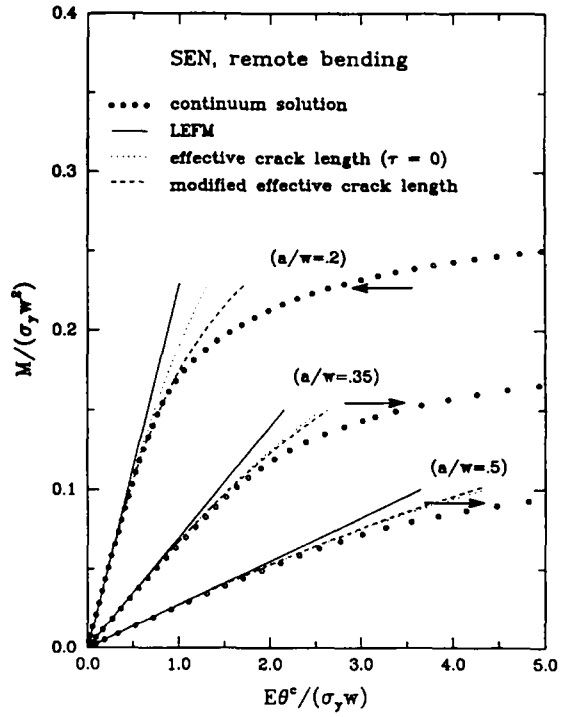


Fig. 8. Normalized bending moment $M$ versus cracked displacement for remote bending of a plane-strain SEN. Horizontal arrows denote limit loads based on $\sigma_y$.

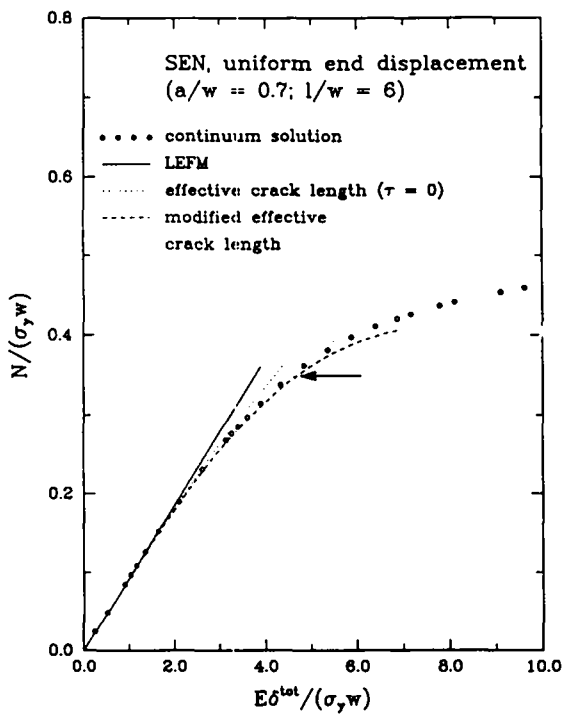


Fig. 9. Normalized axial force $N$ versus total displacement for uniform end displacement of a plane-strain SEN. Horizontal arrow denotes combined loading limit load based on $\sigma_y$ (see also Fig. 17).

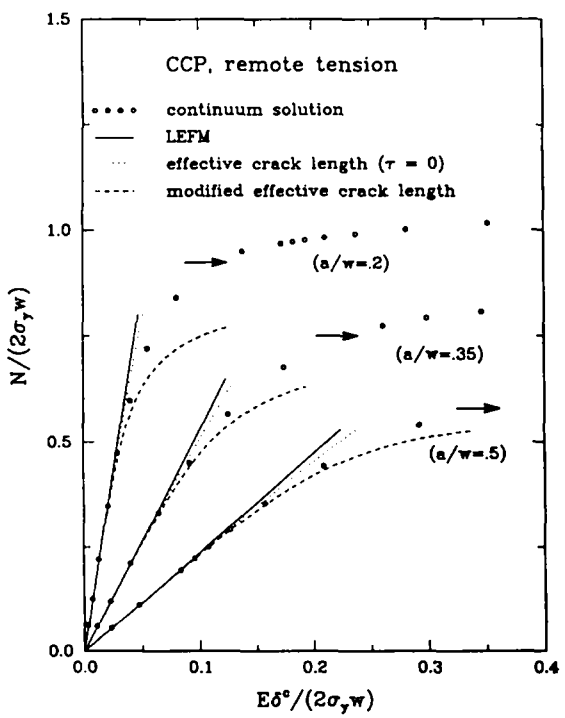


Fig. 10. Normalized axial force $N$ versus cracked displacement for remote tension of a plane-strain CCP. Horizontal arrows denote limit loads based on $\sigma_y$.

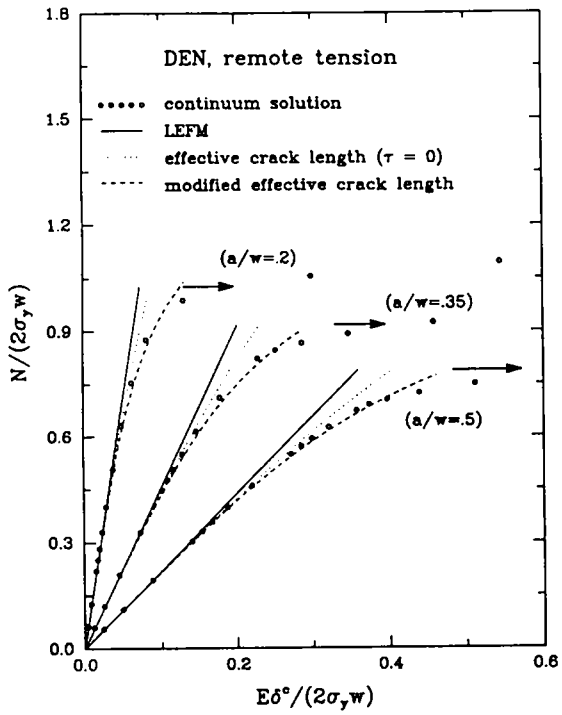


Fig. 11. Normalized axial force $N$ versus cracked displacement for remote tension of a plane-strain DEN. Horizontal arrows denote limit loads based on $\sigma_y$.

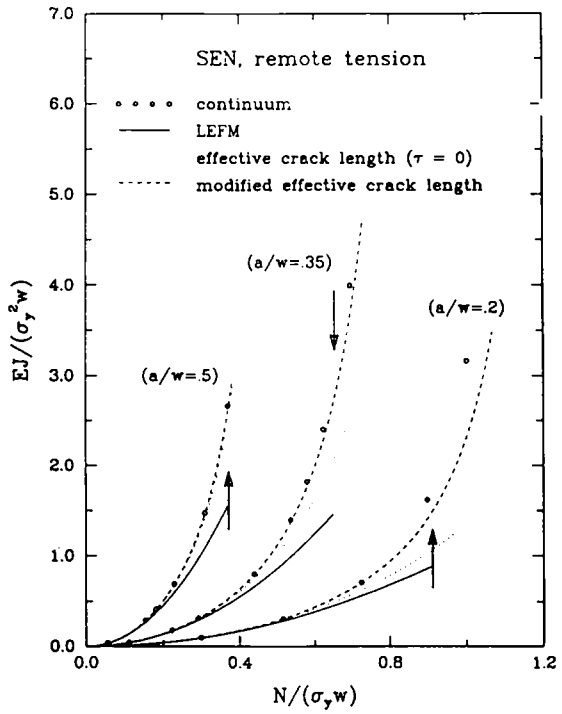


Fig. 12. Normalized $J$ versus axial force $N$ for remote tension of a plane-strain SEN. Vertical arrows denote limit loads based on $\sigma_y$.

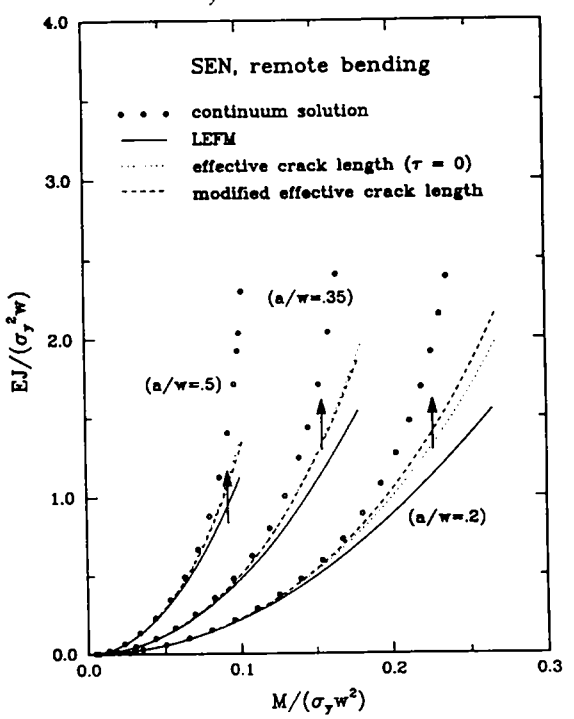


Fig. 13. Normalized $J$ versus bending moment $M$ for remote bending of a plane-strain SEN. Vertical arrows denote limit loads based on $\sigma_y$.

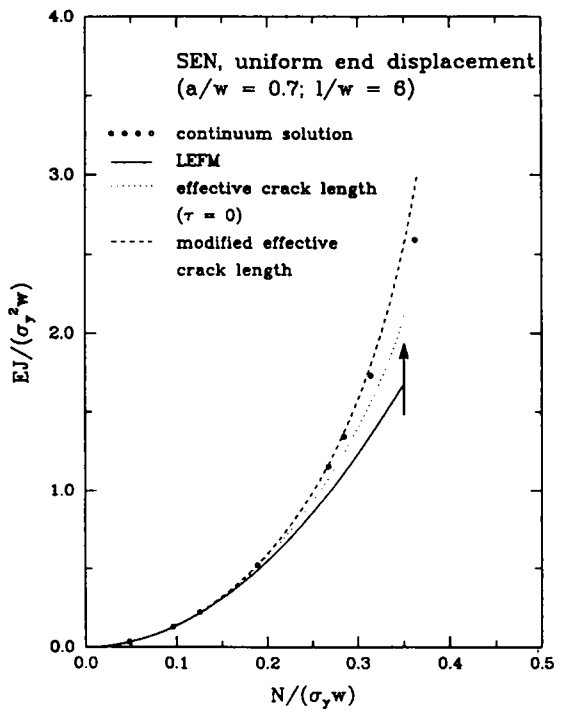


Fig. 14. Normalized $J$ versus axial force $N$ for uniform end displacement of a plane-strain SEN. Vertical arrow denotes combined loading limit load based on $\sigma_y$ (see also Fig. 17).

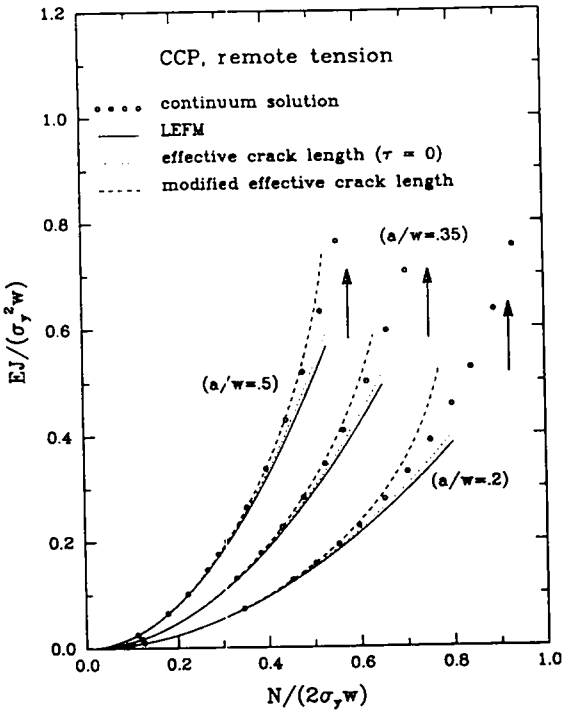


Fig. 15. Normalized $J$ versus axial force $N$ for remote tension of a plane-strain CCP. Vertical arrows denote limit loads based on $\sigma_y$.

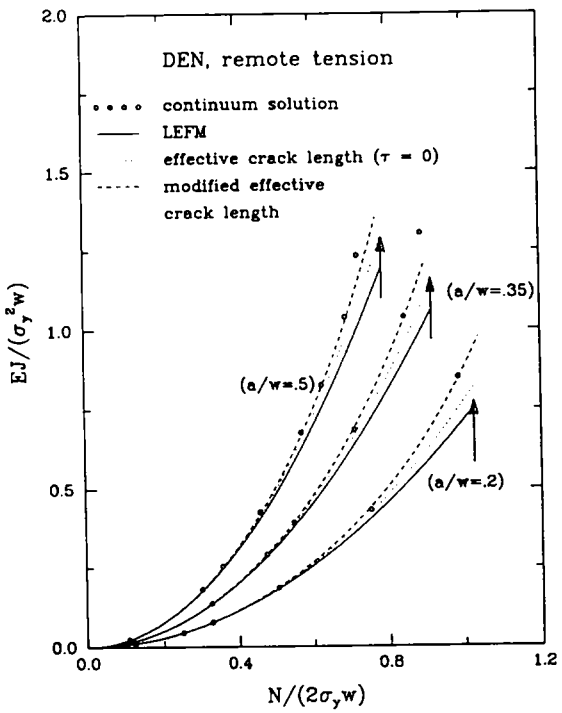


Fig. 16. Normalized $J$ versus axial force $N$ for remote tension of a plane-strain DEN. Vertical arrows denote limit loads based on $\sigma_y$.

Inclusion of the $T$-stress in the standard ECL formulation considerably "improves" the results for all specimens; accurate $J$ versus load and load versus displacement estimates are obtained to higher fractions of limit load in cases of negative $T$-stress without compromising the performance for lower loads or positive $T$-stress cases, both of which cases essentially recover the standard ECL formulation.

The $T$-stress allows the solutions based on the modified effective crack length to separate from both the LEFM and the standard ECL solutions and to follow the continuum solution further into the regime of elastic–plastic transition. For the remote tension cases, this influence of the $T$-stress on estimated compliance seems to be accurate to higher fractions of limit load for the SEN and DEN specimens than for the CCP specimen. The elastic–plastic transition is followed very accurately for the SEN and DEN specimens of all relative crack depths considered (see Figs. 7 and 11). The MECL solutions for the CCP specimen, on the other hand, tend to overcorrect compliance estimates at the highest loads (Fig. 10). The overcorrection is greatest in the shallower CCP specimens which have the most negative $T$-stress at high fractions of limit load.

The relative improvement of $J$-integral estimates for the remote tension cases is evident in Figs. 12, 15 and 16. The results for the SEN specimens of relative crack depths $a/w = 0.5$ and $a/w = 0.35$ and for the DEN specimens of all relative crack depths are exceptional, following the continuum solutions up to and beyond limit load. The solutions for the SEN specimen of relative crack depth $a/w = 0.2$ and for the CCP specimens of all relative crack depths extend the load ranges of accurate solutions well beyond those exhibited by the LEFM and the standard ECL solutions. Slight overcorrections are shown only at the highest loads.

The MECL solutions of the SEN specimen under pure bending show a clear distinction from the standard ECL solutions only for the case of relative crack depth $a/w = 0.2$. The solutions for the specimens of relative crack depths $a/w = 0.35$ and 0.5, which have non-negative $\tau$ at all loads, practically coincide with

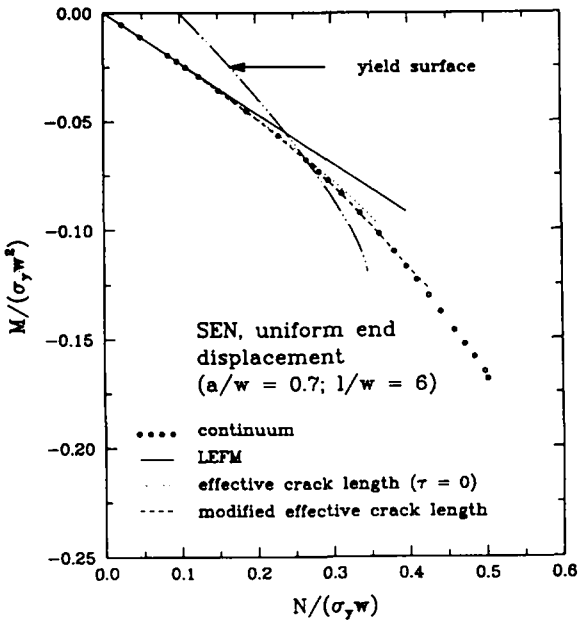


Fig. 17. Normalized axial force $N$ versus bending moment $M$ for uniform end displacement of a plane-strain SEN. Also shown is an upper bound initial yield surface (based on $\sigma_y$) as suggested by Rice (1972b).

the standard ECL solutions, while $\tau$ for the shallow ($a/w = 0.2$) crack in bending grows increasingly negative with increasing load.

Finally, the deeply-cracked SEN specimen ($a/w = 0.7$) under uniform end displacement (Figs. 9, 14, 17) shows excellent agreement with the continuum solutions.

The varying influences of the elastically-calculated $T$-stress with respect to specimen type and relative crack depth can be explained by evaluating $\tau$ for the three specimens at load levels corresponding to a fixed fraction of respective limit load, at varying crack depths. A graph of $\tau$ at 75% of limit load, denoted "$\tau_{0.75}$", is plotted versus normalized crack size in Fig. 18 for the CCP, DEN, and SEN specimens. Values of $\tau_{0.75}$ for the CCP specimen are the most negative of the three specimens, ranging from $-0.71$ for $a/w = 0.2$ to $-0.55$ for $a/w = 0.5$. Values of $\tau_{0.75}$ for the SEN specimen in tension and the DEN specimen are almost equal for $a/w = 0.2$ ($\tau_{0.75} \sim -0.41$). In the case of the SEN specimen, $\tau_{0.75}$ becomes rapidly less negative as $a/w$ increases to 0.5, while for the DEN specimen, only a slight increase to a value of $\tau_{0.75} = -0.33$ at $a/w = 0.5$ can be noted. The values

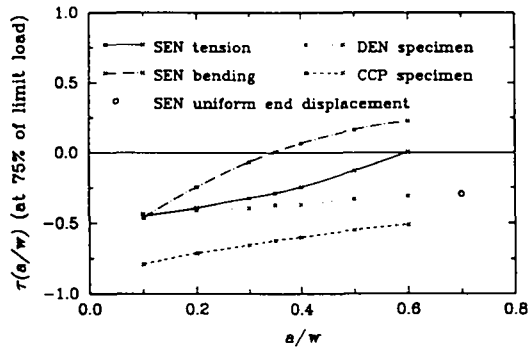


Fig. 18. Variation of $\tau$ at 75% of limit load, termed $\tau_{0.75}$, with relative crack depth, $a/w$, for the SEN, CCP, and DEN specimens.

of $\tau_{0.75}$ for the pure bending case range from $-0.25$ for $a/w = 0.2$ to $0.16$ for $a/w = 0.5$. The value of $\tau_{0.75}$ for the SEN specimen ($a/w = 0.7, l/w = 6$) under uniform end displacement loading is approximately $-0.29$.

## 5. Discussion

In the ongoing efforts aimed at developing two-parameter descriptions of crack-tip fields, the results of this work confirm the $T$-stress as *the* rigorous "second" crack-tip parameter in well-contained yielding (Parks, 1992). It has recently been shown (Betegón and Hancock, 1991; Al-Ani and Hancock, 1991) that the $T$-stress is valuable in characterizing the stress triaxiality of elastic–plastic crack-tip fields. O'Dowd and Shih (1991, 1992) note that, in small- to moderate-scale yielding, their second crack-tip parameter, $Q$ (measuring the deviation in crack-tip stress triaxiality from a particular reference value), is isomorphic to the $T$-stress. Negative $T$-stresses ($\tau < 0$) are associated with a substantial reduction in crack-tip stress triaxiality (compared to SSY), while positive $T$-stresses result in only modest elevation of triaxiality above SSY. This dependence of crack-tip stress triaxiality on $\tau$, along with the marked sensitivity of both ductile (void growth) and brittle (cleavage) fracture mechanisms to stress triaxiality, has profound influences on crack toughness and growth ductility. Al-Ani and Hancock (1991), for example, demonstrated that the deviation from SSY of near tip crack opening stress profiles in plane strain edge-cracked geometries can be accurately predicted by the MBL solution of the respective problems up through (and beyond) moderate-scale

yielding. For such loads, the parameter $\tau$, as elastically calculated based on load level, plus the parameter $J$, as calculated based on the actual elastic–plastic deformation field, rigorously and accurately describe the local crack-tip stress and deformation (Parks, 1992). Hancock et al. (1993) showed how $\tau$ and associated changes in crack-tip stress triaxiality change the initial slopes of resistance curves in A710 specimens of varying geometry. Based on these results, then, it should be emphasized that the approach outlined in this paper not only extends the validity of effective crack length formulations, but also permits accurate implementation of two-parameter ($J$, $T$) fracture mechanics approaches, again, based on only elastic calibration functions for $K_I$ and $T$.

As noted earlier, the effect of the $T$-stress on yield zones of fracture specimens was also investigated by Rice (1974) based on a simple plane-strain shear-band yielding model. In this work, Rice gave a Taylor series expansion of the expression for plastic zone size, Eq. (12), about $T = 0$ at an angle of $\phi = 70.6°$ measured from the crack plane as

$$r_p^{max} = \frac{\pi}{18}\left(\frac{K_I}{\sigma_y}\right)^2\left[1 - \frac{4}{3}\sqrt{\frac{2}{3}}\left(\frac{T}{\sigma_y}\right) + \cdots\right], \tag{26}$$

where the bracketed terms represent the deviation from the SSY approximation.

A Taylor series expansion about $T = 0$ of our approximate expression for the maximum plastic zone size ($r_p^{max} = \rho(\tau, n)\, r_p^{SSY}$) gives

$$r_p^{max} = 0.15\left(\frac{K_I}{\sigma_y}\right)^2\left[1 - 1.241\left(\frac{T}{\sigma_y}\right) + \cdots\right]. \tag{27}$$

Comparison of the respective series coefficients in Eq. (26) and Eq. (27) shows good agreement, which is also evident in Fig. 1.

Edmunds and Willis (1977) noted that the standard ECL plastic zone correction can provide no more than the second term in their asymptotic series for the $J$-integral [of $O(\varepsilon^4)$], as it cannot correctly model interactions between the near- and far-fields.

By comparing Edmunds and Willis' plastic-zone-corrected series expansion for $J$ with their asymptotic series to order $\varepsilon^5$ rather than to $\varepsilon^4$, Willis (1992) recently derived an expression for the effective crack length correction $r_y$ as

$$r_y = 2C_1(n)\gamma_{11}^2\varepsilon^2 + 2\left[C_3(n)\gamma_{11}^2\gamma_{12} + C_2(n)\gamma_{11}^3\frac{(\gamma_{11}\gamma_{44} - \gamma_{14})}{(\gamma_{13} + \gamma_{11}\gamma_{33})}\right]\varepsilon^3, \tag{28}$$

where the $\gamma_{ij}$ are constants defining the near-tip asymptotic form of the linear elastic "outer" solutions (see, e.g., Edmunds and Willis, 1977).

Using Eq. (5) in Eq. (28), the plastic zone correction can be written in terms of the stress intensity factor $K_I$ as

$$r_y = \frac{C_1(n)}{4\pi}\left(\frac{K_I}{\sigma_y}\right)^2\left[1 + \frac{C_3(n)}{4C_1(n)}\left(\frac{T}{\sigma_y}\right) + O(\varepsilon)\right], \tag{29}$$

where we have used the fact that $4\gamma_{12}\varepsilon = T/\sigma_y$. The term of $O(\varepsilon)$ contains the ratio of the rates of change with $a$ of $T$ and $K_I$; i.e.,

$$\gamma_{13} + \gamma_{11}\gamma_{33} = 2\frac{\partial\gamma_{11}}{\partial a}, \tag{30}$$

$$\gamma_{11}\gamma_{44} - \gamma_{14} = -\frac{\partial\gamma_{12}}{\partial a}. \tag{31}$$

For a power-law hardening material ($n = 10$) satisfying the Mises yield criterion $C_1|_{n=10} = 0.2$ and $C_3|_{n=10} = -0.68$ (Edmunds and Willis, 1977), and the plastic zone correction becomes

$$r_y = 0.0159\left(\frac{K_I}{\sigma_y}\right)^2 \times\left[1 - 0.85\left(\frac{T}{\sigma_y}\right) + O(\varepsilon)\right]. \tag{32}$$

A two-term Taylor series expansion of $\rho(\tau)$ about $T = 0$ in Eq. (17) allows direct comparison with this expression; i.e.,

$$r_{y,mod} = 0.0195\left(\frac{K_I}{\sigma_y}\right)^2 \times\left[1 - 1.241\left(\frac{T}{\sigma_y}\right) + O(\varepsilon^2)\right]. \tag{33}$$

The difference in the leading coefficients of Eqs. (32) and (33) is acceptable in view of the range

of coefficients reported in the literature. Acknowledging this difference, the coefficients of the second term agree reasonably well, not only in sign but also in magnitude. Notice that the third term in Eq. (32) is of $O(\varepsilon)$ compared to $O(\varepsilon^2)$ in Eq. (33). Thus, agreement of the second term coefficients also depends on the geometry of the specimen under consideration [cf. Eqs. (30) and (31)]; we have not pursued the effect of including these neglected terms on the performance which can be obtained from a restricted form of the Edmunds–Willis approach. However, in all geometries characterized by a single length dimension, the $O(\varepsilon)$ term must vanish on dimensional grounds, and may be small for many other cases.

At higher loads in shallow-cracked CCP specimens, there is a strong interaction between the growing crack-tip plastic zones and the rigid kinematic condition at the nearby vertical symmetry plane. In the elastic Griffith configuration ($a/w \to 0$), the compressive traction across the centerline on the crack faces numerically equals the negative $T$-stress. Continuum finite-element simulations of CCP specimens having $a/w = 0.1$ (Wang and Parks, 1995) have shown how increasing crack-tip plasticity changes the distribution of $\sigma_{xx}(x = 0; y)$ in the region $|y| \leq a$. In particular, the centerline traction becomes less negative than the elastically-calculated value of $T$. The changing traction distributions, in conjunction with a weight function for $T$-stress (Sham, 1991), permitted Wang and Parks (1995) to define an "effective" $T$-stress for the CCP specimen which at large yielding was less negative than the elastically calculated value for the CCP geometry. Use of such a less negative "effective" value for $T$ in the current model would tend to bring the curves of Fig. 10 into closer agreement with the continuum solutions, but would be counter to the spirit of the very simple MECL procedure offered here. More involved numerical procedures taking into account the interaction of plastic zones with the remote structural elastic domains (e.g., Edmunds and Willis, 1986) provide formal means for extending the loading range of accurate calculation even in cases of strong interaction as in the CCP specimens. Evidently, the "strength" of such interactions is less in SEN and DEN geometries considered here.

In summary, the new formulation consistently extends the load range for which accurate predictions of compliance, $J$-integral, and crack-tip constraint are obtained in several plane strain specimen geometries. The magnitude of influence of the $T$-stress varies with specimen type and relative crack depth. The greatest "improvement" to standard effective crack length approximations occurs in specimens of "moderately" negative $T$-stress.

## Acknowledgements

This work was supported by the Office of Basic Energy Sciences, Department of Energy, under Grant # DE-FG02-85ER13331. Computations were performed on SunSparc workstations obtained under ONR Grant # 0014-89-J-3040. The ABAQUS finite-element program (Hibbitt et al., 1988) was made available under academic license from Hibbitt, Karlsson and Sorensen, Inc., Pawtucket, RI. D.M.P. is pleased to acknowledge the useful discussions and interactions with Professors R.M. McMeeking and J.R. Willis. We thank Prof. T.-L. Sham for access to data on the $T$-stress calibration functions.

## References

Al-Ani, A.M. and J.W. Hancock (1991), *J*-Dominance of Short Cracks in Tension and Bending, *J. Mech. Phys. Solids 39(1)*, 23–43.

ASTM (1983), Standard test method for plane-strain fracture toughness of metallic materials, *Annual Book of ASTM Standards, E399-83*, American Society for Testing and Materials, Philadelphia, PA.

Betegón, C. and J.W. Hancock (1991), Two-parameter characterization of elastic-plastic crack-tip fields, *J. Appl. Mech. 58*, 104–110.

Edmunds, T.M. and J.R. Willis (1977), Matched asymptotic expansions in nonlinear fracture mechanics – III. In-plane loading of an elastic perfectly-plastic symmetric specimen, *J. Mech. Phys. Solids 25*, 423–455.

Edmunds, T.M. and J.R. Willis (1986), Fracture characterizing parameters in linear and non-linear fracture mechanics, in: A.S. Tooth and J. Spence, eds., *Applied Solid Mechanics – 1*, Elsevier Applied Science Publishers, London, pp. 41–57.

Hancock, J.W., W.G. Reuter and D.M. Parks (1993), Constraint and toughness parameterized by $T$, E.M. Hackett, K.-H. Schwalbe and R.H. Dodds, eds., *Constraint Effects in Fracture, ASTM STP 1171*, American Society for Testing and Materials, Philadelphia, pp. 21–40.

Harlin, G. and J.R. Willis (1988), The influence of crack size on the ductile-brittle transition, *Proc. R. Soc. London A 415*, 197–226.

Hibbitt, Karlsson and Sorensen, Inc. (1988), *ABAQUS User's Manual*, version 4.9, Hibbitt, Karlsson and Sorensen, Inc., Pawtucket, RI.

Hilton, P.D. and J.W. Hutchinson (1971), Plastic intensity factors for cracked plates, *Eng. Fracture Mech. 3*, 435–451.

Hult, J.A. and F.A. McClintock (1956), Elastic-plastic stress and strain distribution around sharp notches under repeated shear, *IXth International Congress for Applied Mechanics*, Brussels, Vol. 8, pp. 51–62.

Irwin, G.R. (1958), Fracture, in: S. Flügge, eds., *Handbuch der Physik VI*, pp. 551–590, Springer, Berlin.

Larsson, S.G. and A.J. Carlsson (1973), Influence of non-singular stress terms and specimen geometry on small-scale yielding at crack tips in elastic-plastic material, *J. Mech. Phys. Solids 21*, 263–277.

Lee, H. and D.M. Parks (1995), Enhanced elastic-plastic line-spring finite element, *Int. J. Solids Struct.*, in press.

Leevers, P.S. and J.C. Radon (1982), Inherent stress biaxiality in various fracture specimen geometries, *Int. J. Fracture 19*, 311–325.

O'Dowd, N.P. and C.F. Shih (1991), Family of crack-tip fields characterized by a triaxiality parameter – I. Structure of fields, *J. Mech. Phys. Solids 39(8)*, 989–1015.

O'Dowd, N.P. and C.F. Shih (1992), Family of crack-tip fields characterized by a triaxiality parameter – II. Fracture applications, *J. Mech. Phys. Solids 40(5)*, 939–963.

Parks, D.M. (1992), Advances in characterization of elastic-plastic crack-tip fields, in: A.S. Argon, eds., *Topics in Fracture and Fatigue, McClintock Festschrift*, Springer Verlag, New York, pp. 58–98.

Rice, J.R. (1972a), Some remarks on elastic crack tip fields, *Int. J. Solids Struct. 8*, 751–758.

Rice, J.R. (1972b), The line-spring model for surface flaws, in: J.L. Swedlow, eds., *The Surface Crack: Physical Problems and Computational Solutions* American Society of Mechanical Engineers, New York, pp. 171–185.

Rice, J.R. (1974), Limitations to the small-scale yielding approximation for crack tip plasticity, *J. Mech. Phys. Solids 22*, 17–26.

Sham, T.-L. (1984), A finite-element study of the asymptotic near-tip fields for mode I plane-strain cracks growing stably in elastic-ideally plastic solids, in: C.F. Shih and J.P. Gudas, eds., *Elastic-Plastic Fracture: Second Symposium, Volume I – Inelastic Crack Analysis, ASTM STP 803*, American Society for Testing and Materials, (1983), pp. I-52–I-79.

Sham, T.-L. (1991), The determination of the elastic $T$-term using higher order weight functions, *Int. J. Fracture 48*, 81–102.

Sham, T.-L. (1992), private communication.

Shih, C.F., N.P. O'Dowd and M.T. Kirk (1993), A framework for quantifying crack tip constraint, in: E.M. Hackett, K.-H. Schwalbe and R.H. Dodds, eds., *Constraint Effects in Fracture, ASTM STP 1171* American Society for Testing and Materials, Philadelphia, pp. 2–20.

Tada, H., P.C. Paris and G.R. Irwin (1985), *The Stress Analysis of Cracks Handbook* (2nd Ed.), Fracture Proof Design, Saint Louis, MO.

Wang, Y.-Y. (1991), A two-parameter characterization of elastic-plastic crack-tip fields and applications to cleavage fracture, Ph.D. Thesis, Department of Mechanical Engineering, Massachusetts Institute of Technology, September, 1991.

Wang, Y.-Y. and D.M. Parks (1992), Evaluation of the elastic $T$-stress in surface-cracked plates using the line-spring method, *Int. J. Fracture 56*, 25–40.

Wang, Y.-Y. and D.M. Parks (1995), Limits of $J$-$T$ characterization of elastic-plastic crack-tip fields, in: M.T. Kirk and A. Bakker, eds. *Constraint Effects in Fracture: Theory and Applications*, presented at ASTM Symposium on Dallas, November, 1993; *ASTM STP 1244*, in press

Williams, M.L. (1957), On the stress distribution at the base of a stationary crack, *J. Appl. Mech. 24*, 111–114.

Willis, J.R. (1992), private communication.

## Appendix A

From Eq. (24), we can write

$$\mathrm{d}\boldsymbol{q}^{\mathrm{crack}} = \left[\int_0^a \frac{\partial^2 J(\boldsymbol{Q}, a^*)}{\partial \boldsymbol{Q}^2}\,\mathrm{d}a^*\right]\mathrm{d}\boldsymbol{Q}, \tag{A.1}$$

where

$$\frac{\partial^2 J(\boldsymbol{Q}, a^*)}{\partial \boldsymbol{Q}^2} = \left[\frac{\partial K_{\mathrm{eff}}}{\partial \boldsymbol{Q}} \otimes \frac{\partial K_{\mathrm{eff}}}{\partial \boldsymbol{Q}} + K_{\mathrm{eff}}\frac{\partial^2 K_{\mathrm{eff}}}{\partial \boldsymbol{Q}^2}\right]\frac{2}{E'}. \tag{A.2}$$

From Eqs. (A.1) and (A.2), the Jacobian matrix is given by

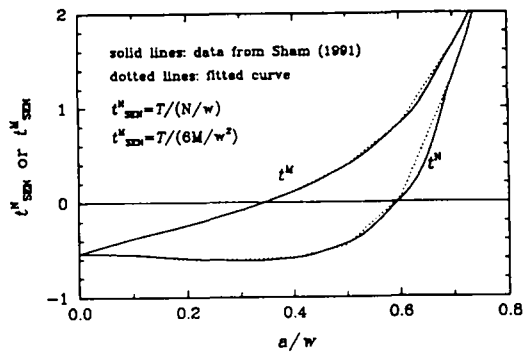


Fig. B.1. $T$-stress calibration functions of single edge-cracked specimen under tension and bending (Wang and Parks, 1992).

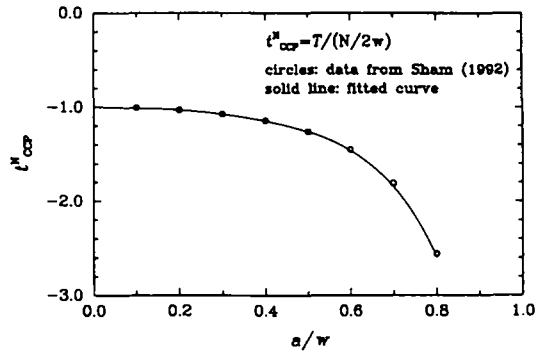


Fig. B.2. $T$-stress calibration function of center-cracked specimen under tension (Sham, 1992).

$$\frac{\partial Q}{\partial q^{\text{crack}}} = \left[\int_0^a \left(\frac{\partial K_{\text{eff}}}{\partial Q} \otimes \frac{\partial K_{\text{eff}}}{\partial Q} + K_{\text{eff}} \frac{\partial^2 K_{\text{eff}}}{\partial Q^2}\right) da^*\right]^{-1} \frac{E'}{2}. \tag{A.3}$$

The partial derivatives in Eq. (A.3) are obtained by making use of Eq. (10). Thus,

$$\frac{\partial K_{\text{eff}}(Q,a^*)}{\partial Q} = \hat{k}(a_{\text{eff}}(Q,a^*)) + \left(\hat{k}'(a_{\text{eff}}(Q,a^*)) \cdot Q\right) \frac{\partial a_{\text{eff}}}{\partial Q}, \tag{A.4}$$

and

$$\begin{aligned}\frac{\partial^2 K_{\text{eff}}(Q,a^*)}{\partial Q^2} &= \hat{k}'(a_{\text{eff}}(Q,a^*)) \otimes \frac{\partial a_{\text{eff}}}{\partial Q} + \frac{\partial a_{\text{eff}}}{\partial Q} \otimes \hat{k}'(a_{\text{eff}}(Q,a^*)) \\ &+ \left(\hat{k}''(a_{\text{eff}}(Q,a^*)) \cdot Q\right)\left[\frac{\partial a_{\text{eff}}}{\partial Q} \otimes \frac{\partial a_{\text{eff}}}{\partial Q}\right] + \left(\hat{k}'(a_{\text{eff}}(Q,a^*)) \cdot Q\right) \frac{\partial^2 a_{\text{eff}}}{\partial Q^2},\end{aligned} \tag{A.5}$$

where the prime denotes differentiation with respect to $a_{\text{eff}}$. The partial derivative of the effective crack length with respect to the load is given as

$$\frac{\partial a_{\text{eff}}}{\partial Q} = \frac{\eta_1 + \eta_2}{c - \tau'(a_{\text{eff}})(\partial \rho(\tau(a_{\text{eff}}))/\partial \tau) K_{\text{I}}^2(\hat{a}_{\text{eff}})}, \tag{A.6}$$

where $\tau'(a_{\text{eff}}) = (1/\sigma_y)\,(\hat{t}'(a_{\text{eff}}) \cdot Q)$, $c = \sigma_y^2/\lambda(n)$, and

$$\eta_1 = \hat{t}(a_{\text{eff}}) \frac{\partial \rho(\tau(a_{\text{eff}}))}{\partial \tau} \frac{K_{\text{I}}^2(\hat{a}_{\text{eff}})}{\sigma_y} \qquad \eta_2 = 2\rho(\tau(a_{\text{eff}})) K_{\text{I}}(\hat{a}_{\text{eff}}) \frac{\partial K_{\text{I}}(\hat{a}_{\text{eff}})}{\partial Q}.$$

## Appendix B

Wang (1991) fitted Sham's data points ($0.1 \le a/w \le 0.9$) for the SEN specimen shown in Fig. B.1 in the range of $0 \le a/w \le 0.8$ with a fourth-order polynomial function, yielding:

$$\hat{t}_{\text{SEN}}\left(\frac{a_{\text{eff}}}{w}\right) = b_0 + b_1\left(\frac{a_{\text{eff}}}{w}\right) + b_2\left(\frac{a_{\text{eff}}}{w}\right)^2 + b_3\left(\frac{a_{\text{eff}}}{w}\right)^3 + b_4\left(\frac{a_{\text{eff}}}{w}\right)^4, \tag{B.1}$$

where $(b_0, b_1, b_2, b_3, b_4) = (-0.501, -1.842, 14.48, -45.03, 47.42)$ for $\hat{t}^N_{\text{SEN}} \equiv T/(N/w)$ in tension and $(b_0, b_1, b_2, b_3, b_4) = (-0.505, 0.906, 3.637, -10.73, 14.08)$ for $\hat{t}^M_{\text{SEN}} \equiv T/(6M/w^2)$ in bending. The limiting

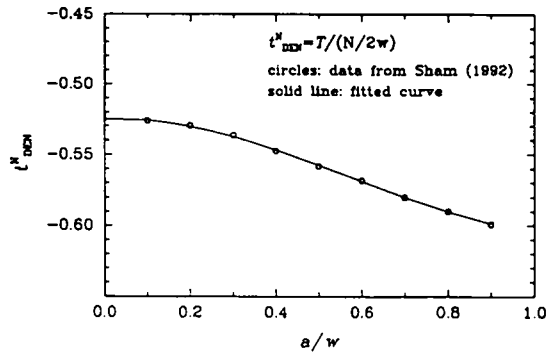


Fig. B.3. $T$-stress calibration function of double edge-cracked specimen under tension (Sham, 1992).

value as $a/w \to 0$ was estimated as $\hat{t}^N_{SEN}(a_{eff}/w) = \hat{t}^M_{SEN}(a_{eff}/w) \to\sim -0.51$ from a finite-element result (Harlin and Willis, 1988) and supplemented to Sham's data set to obtain the results.

In the same way, we fitted the data points for the CCP specimen (Fig. B.2) in the range of $0 \leq (a/w) \leq 0.8$ with a fifth-order polynomial function:

$$\hat{t}^N_{CCP}\left(\frac{a_{eff}}{w}\right) \equiv \frac{T}{(N/2w)} = d_0 + d_1\left(\frac{a_{eff}}{w}\right) + d_2\left(\frac{a_{eff}}{w}\right)^2 + d_3\left(\frac{a_{eff}}{w}\right)^3 + d_4\left(\frac{a_{eff}}{w}\right)^4 + d_5\left(\frac{a_{eff}}{w}\right)^5, \tag{B.2}$$

where $(d_0, d_1, d_2, d_3, d_4, d_5) = (-1.0, -0.305, 2.816, -15.539, 28.455, -20.937)$. The value $d_0 = -1.0$ at $a_{eff}/w = 0$ corresponds to the analytical result for a Griffith crack under uniaxial tension; i.e., $T = \hat{t}^N_{CCP}(a_{eff}/w)|_{a_{eff}/w=0}\sigma^{nom} = -\sigma^{nom}$, where $\sigma^{nom} = N/(2w)$.

The data points for the DEN specimen were fitted with a third-order polynomial in the range $0.1 \leq a/w \leq 0.9$ (Fig. B.3),

$$\hat{t}^N_{DEN}\left(\frac{a_{eff}}{w}\right) \equiv \frac{T}{(N/2w)} = e_0 + e_1\left(\frac{a_{eff}}{w}\right) + e_2\left(\frac{a_{eff}}{w}\right)^2 + e_3\left(\frac{a_{eff}}{w}\right)^3, \tag{B.3}$$

where $(e_0, e_1, e_2, e_3) = (-0.525, 0.01, -0.212, 0.122)$, $T = \hat{t}^N_{DEN}\, N/(2w)$. Analytically, $e_0$ for the asymptotically-shallow DEN specimen at $a_{eff}/w \to 0$ should also recover the result ($e_0 = -0.51$) of Harlin and Willis (1988) and the fitting value of $e_0 = -0.525$ is sufficiently close.